Supporting Information

Toward High Practical Capacitance of $Ni(OH)_2$ Using Highly Conductive CoB Nanochain Supports

Hui Wang,[a,+] Jingjing Yan,[a,+] Rongfang Wang,*[a] Shunxi Li,[a] Dan J.L Brett,[b] Julian Key,[c] and Shan Ji*[a,b]

[a] College of Chemistry and Chemical Engineering, Northwest Normal University, Lanzhou, 730070, China, *E-mail: wangrf@nwnu.edu.cn

[b] EIL, Dept. Chemical Engineering, University College London, London WC1E 7JE, UK, *E-mail: shan.ji@ucl.ac.uk

[c] Collaborative Innovation Center of Renewable Energy Materials (CICREM), Guangxi University Guangxi Univerisity, Nanning, 530004, China.

+Equal contributors

Experimental

Material synthesis:

All reagents were of analytic grade, and double-distilled water was used throughout the experiments. To prepare the linear structured CoB sample, 0.35 mmol $CoCl_2 \cdot 6H_2O$ and 0.7 mmol NaOH were dissolved into 35 mL deionized water with intense stirring. Then 35 mL of 0.02 mol $L^{-1}NaBH_4$ solution was added drop-wise to the above solution with the fixed magnetic field intensity of ca. 0.4 Tesla under the vessel. The as-prepared CoB was rinsed with double-distilled water and ethanol alternately, and finally dried in vacuum oven at 40 °C for 8 h.

To prepare $CoB@Ni(OH)_2$, 20 mg of the as-prepared CoB was added to 20 mL deionized water, after which 0.1 mmol $NiCl_2 \cdot 6H_2O$ was dissolved into the suspension. The suspension was stirred at a rotation rate of 500 rpm for 1 h, wherein the following reactions occur:

$Ni^{2+} + Co \rightarrow Ni + Co^{2+}$

$2Ni + O_2 + 2H_2O \rightarrow 2Ni(OH)_2$

The product was rinsed with double-distilled water and ethanol alternately, and finally dried in vacuum oven at 40 °C for 8 h.

Characterization

XRD patterns were recorded on a Shimadzu XD–3A (Japan) using filtered Cu-Kα radiation (λ = 0.15418 nm) generated at 40 kV and 30 mA. Scans for 2θ values were recorded at 4° min^{-1}. Scanning electron microscopy (SEM) images were obtained using a Carl Zeiss Ultra Plus electron microscope. Transmission electron microscopy (TEM) high angle annular dark field scanning transmission electron microscopy (STEM) images of the catalysts were obtained using a JEOL (JEM-2000 FX) microscope operating at 200 kV. Specific surface area was determined by the Brunauer-Emmett-Teller (BET) method, and the density functional theory DFT method was employed for analyzing the full range of pore size distribution based on the sorption isotherms obtained on a Quantachrome Autosorb-1 volumetric analyzer. X-Ray Photoelectron Spectroscopy (XPS) spectra were generated using Thermo Scientific Escalab 250Xi. Binding energies were determined by referencing to the C 1 s peak at 285.0 eV. The molar ratios of Co, B Ni, in the bulk samples were determined by a Varian 720 Inductively Coupled Plasma-Optical Emission Spectrometer (ICP-OES).

Electrochemical measurements

Cyclic voltammograms (CV) and galvanostatic charge/discharge tests on CoB@$Ni(OH)_2$ were carried out in a three-electrode cell. The working electrode comprised 1 cm^2 of a film containing CoB@$Ni(OH)_2$, carbon black and poly(tetrafluoroethylene) with a mass ratio of 80:10:10, pressed into the Ni foam current collectors. An Hg/HgO (1.0 M KOH) reference electrode and an activated carbon counter electrode was used in all experiments in 6 mol L^{-1} KOH electrolyte. CV tests were done on a CHI 650D electrochemical workstation.

Galvanostatic charge/discharge tests were carried out on a Neware Battery Tester (BTS6.0, Neware Technology Company, Guangdong, China).

The capacitance of the electrode (C) was calculated according to the following equation based on CVs or the discharge curves.

$$C = \frac{Q}{V} = \frac{i\Delta t}{\Delta V m} \qquad (1)$$

where i is the sampled current, Δt is a sampling time span, ΔV is the total potential deviation of the voltage window, and m is the mass of the active material examined.

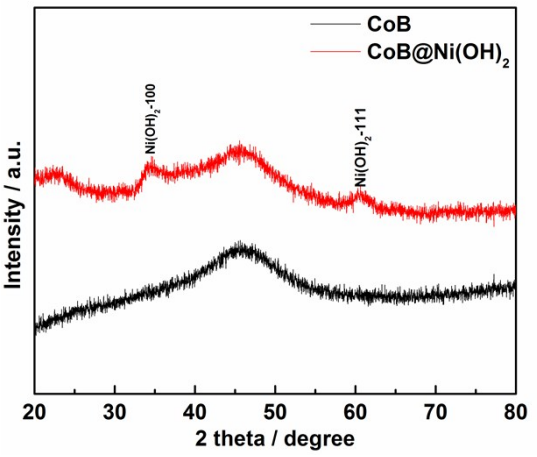

Fig. S1 XRD patterns of CoB and CoB@$Ni(OH)_2$.

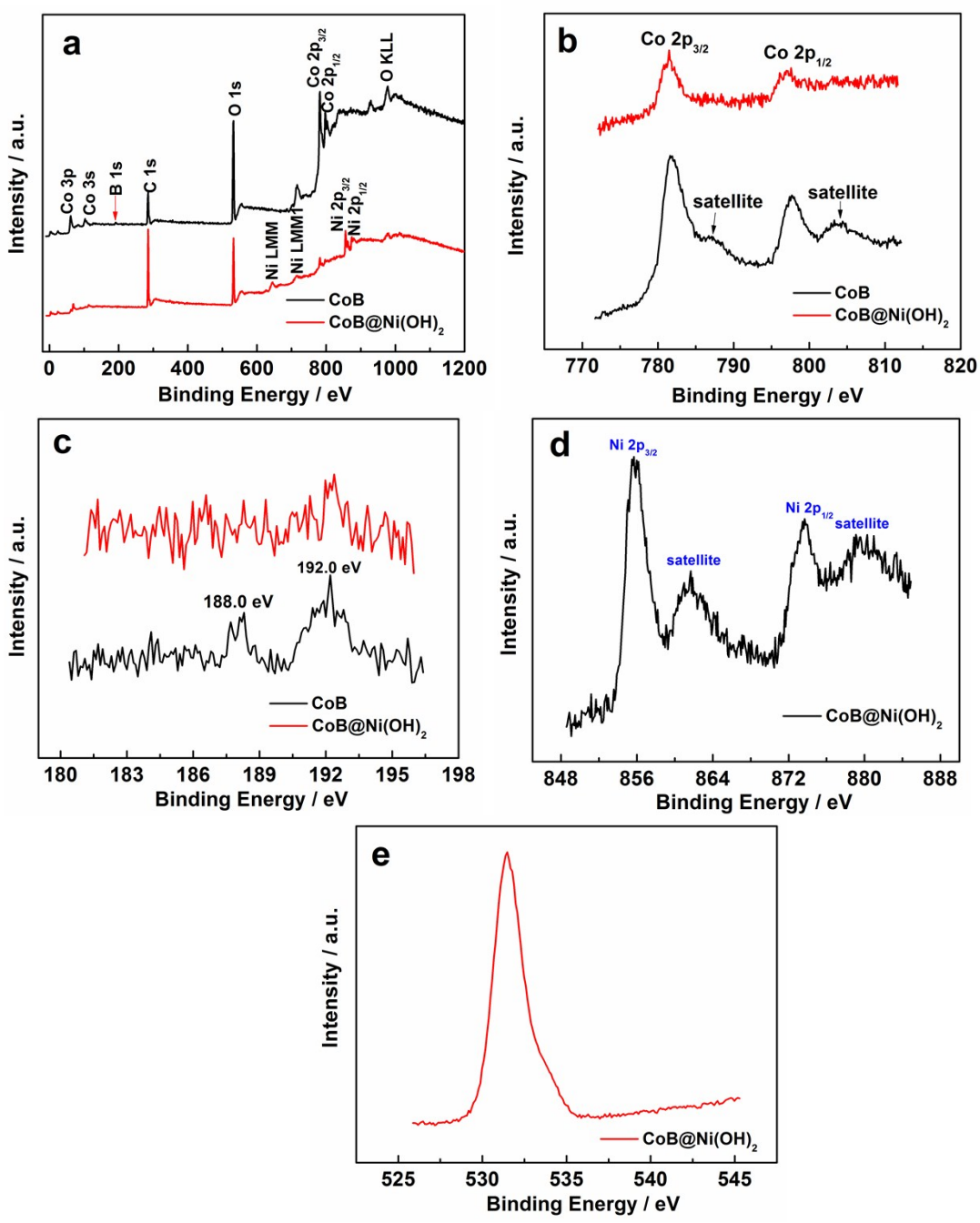

Fig. S2 (a) Overall XPS surveys of CoB and CoB@$Ni(OH)_2$; (b) Co 2p; (c) B 1s XPS of CoB and CoB@$Ni(OH)_2$; (d) Ni 2p; and (e) O 1s XPS of CoB@$Ni(OH)_2$.

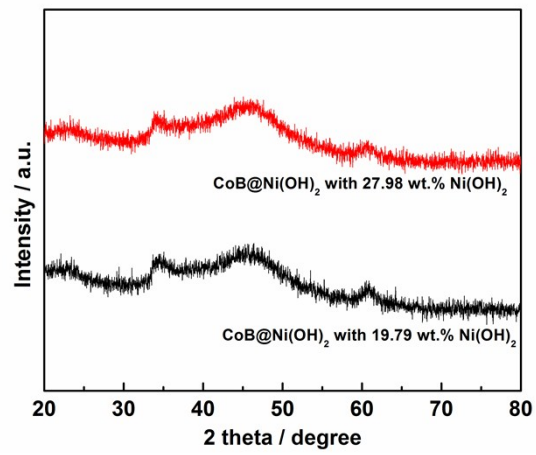

Fig. S3 XRD pattern of CoB@$Ni(OH)_2$ with 19.79 wt.% and 27.98 wt.% $Ni(OH)_2$.

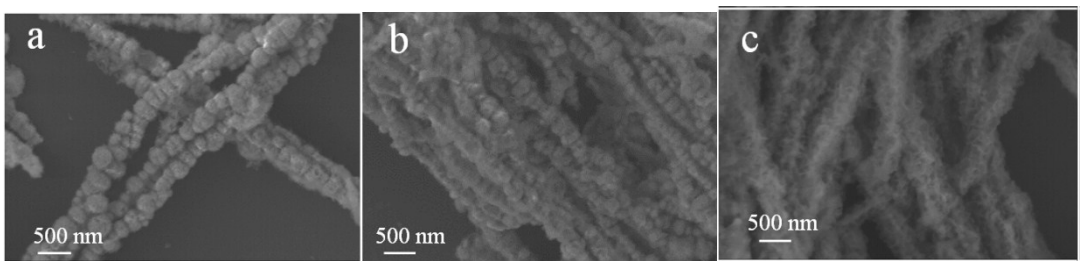

Fig. S4 SEM images of CoB@$Ni(OH)_2$ with the different masses of $Ni(OH)_2$; (a): 12.26 wt.%, (b): 19.79 wt.%, (c): 27.98 wt.%.

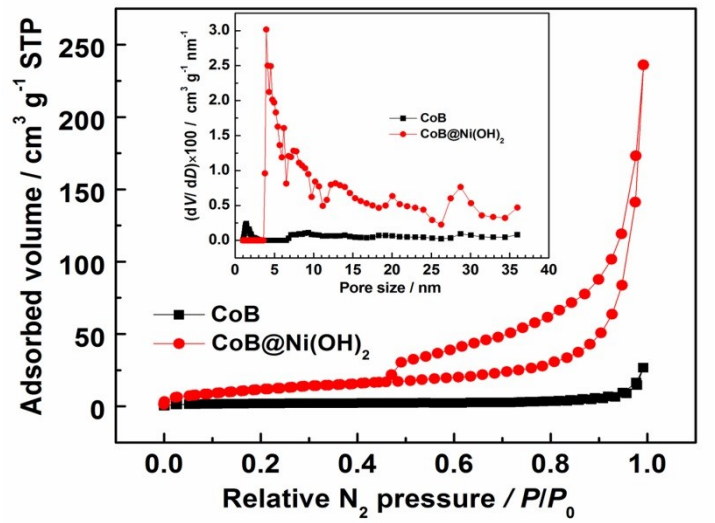

Fig. S5 N_2 isotherms and the pore size distribution (Inset) of CoB and CoB@$Ni(OH)_2$.

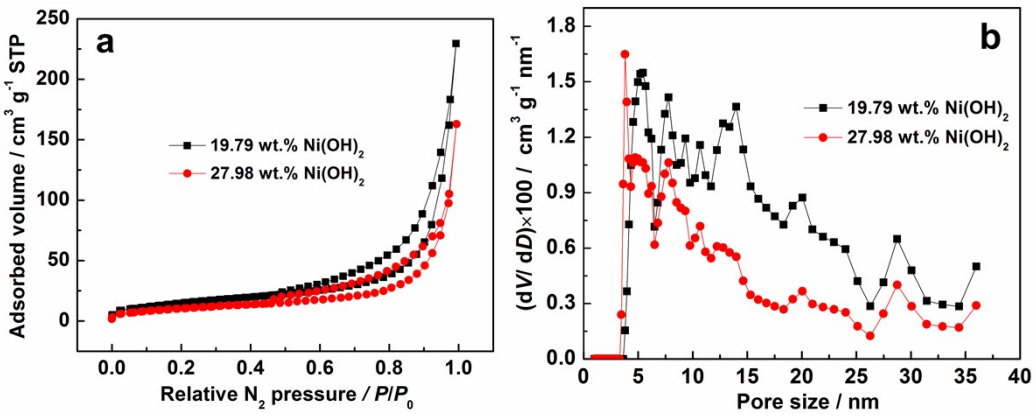

Fig. S6 (a) N_2 isotherms; (b) corresponding pore size distribution of CoB and CoB@Ni(OH)$_2$ with 19.79 wt.% Ni(OH)$_2$ (black line) and 27.98 wt.% Ni(OH)$_2$ (red line).

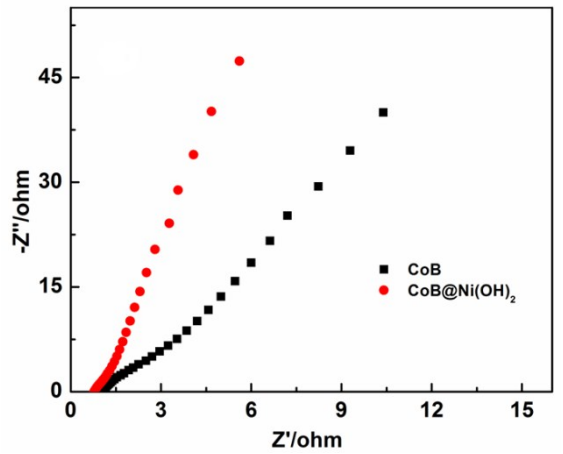

Fig. S7 Comparison of Nyquist plots of the CoB and CoB@Ni(OH)$_2$ (27.98 wt.%) electrodes

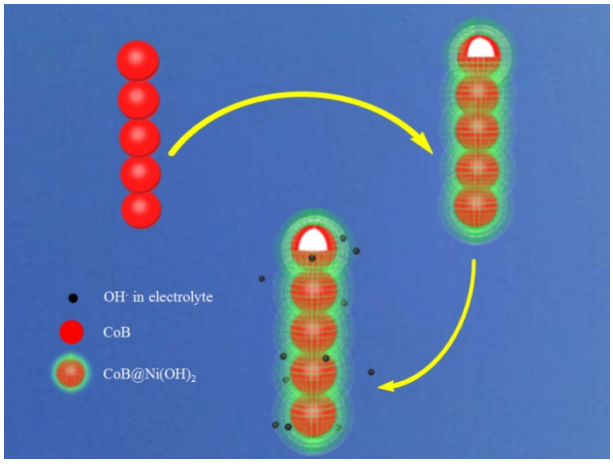

Fig. S8 Schematic of the CoB@Ni(OH)$_2$ hybrid, showing CoB core and Ni(OH)$_2$.

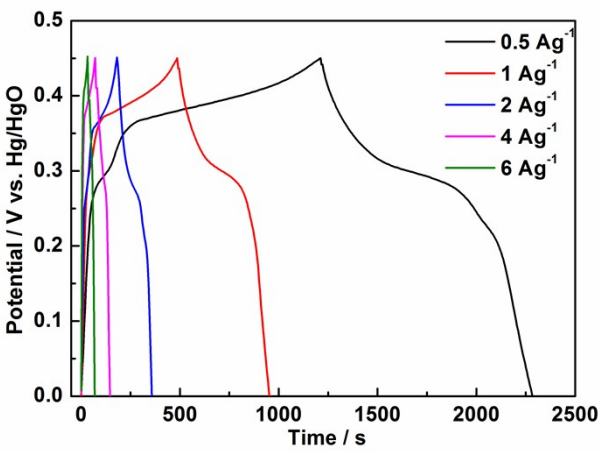

Fig. S9 Galvanostatic charge-discharge curves of CoB at different current densities (0.5, 1, 2, 4, and 6 A g^{-1}).

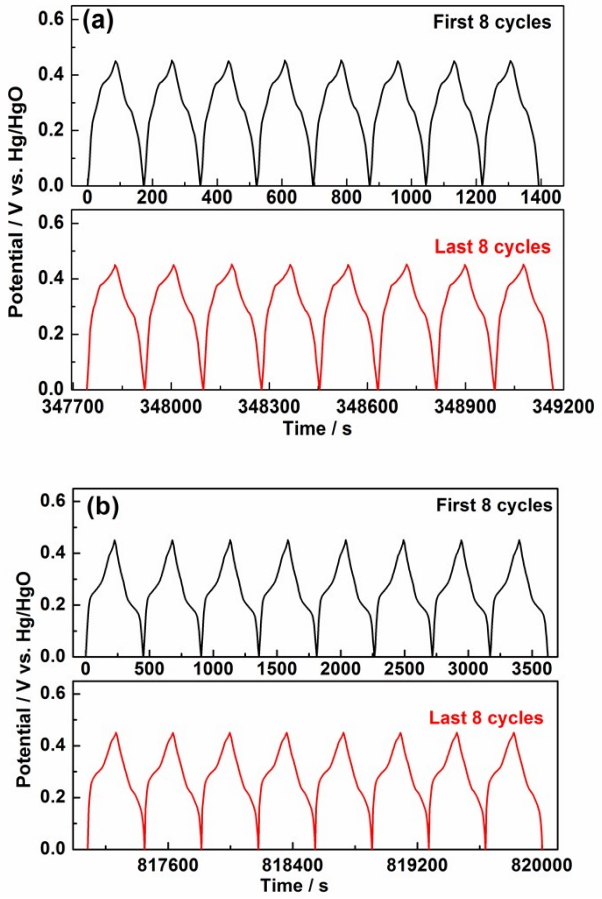

Fig. S10 Charge–discharge curves comparison of the first and last 8 cycles of (a) CoB; and (b) CoB@$Ni(OH)_2$; current density: 2 A g^{-1}; electrolyte: 6 mol L^{-1} KOH.

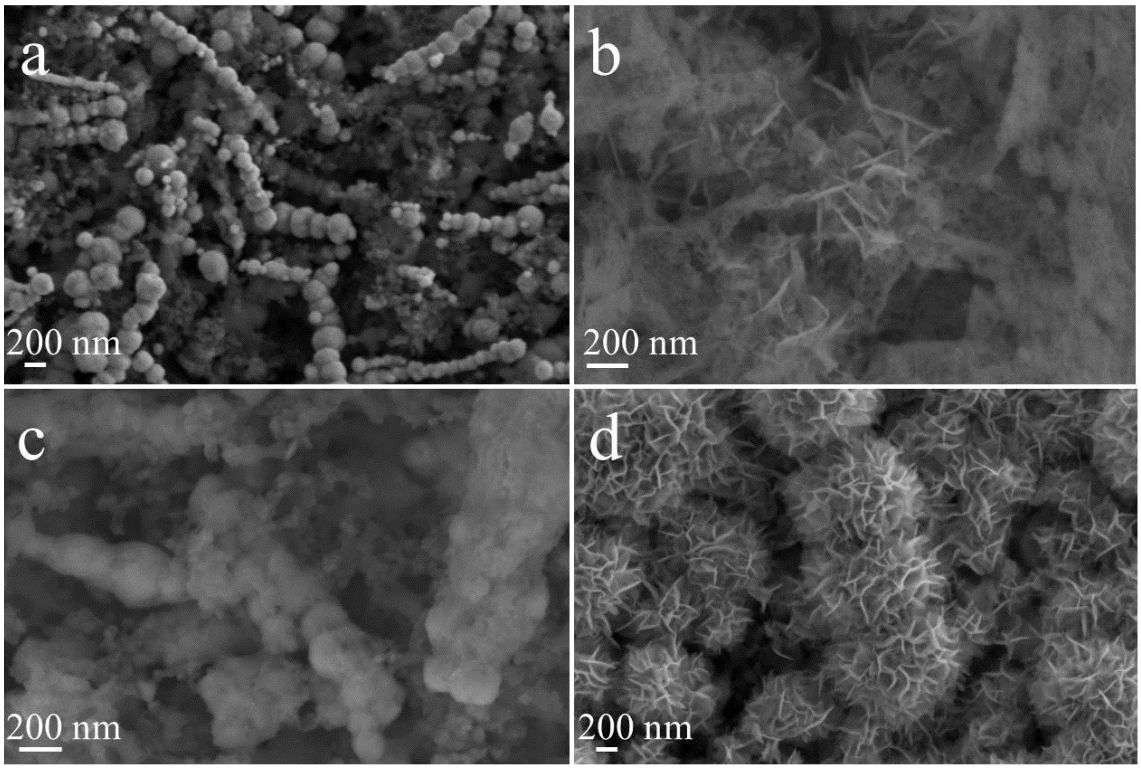

Fig. S11 SEM images of CoB@Ni(OH)$_2$ before (a,b) and after (c,d) 2500 continuous charge-discharge cycles at a current density of 2 A g^{-1}.

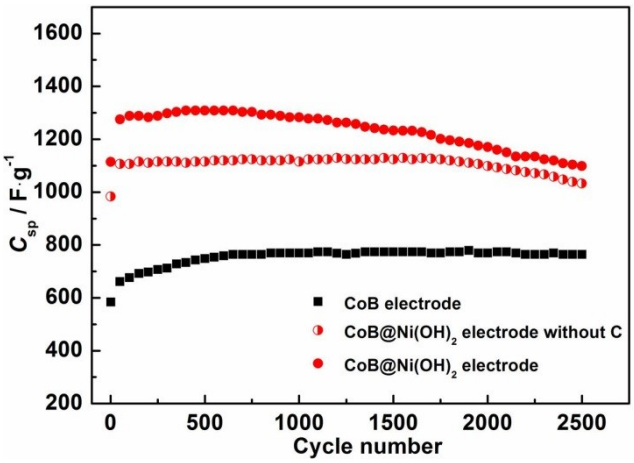

Fig. S12 Cycling tests of the CoB, CoB@Ni(OH)$_2$ and CoB@Ni(OH)$_2$ without carbon electrodes for 2500 cycles at a current density of 2 A g^{-1}.

Table S1. Bulk composition of the as-prepared CoB and a series of CoB@$Ni(OH)_2$ samples.

Sample	Moles of $NiCl_2$ precursor (mmol)	Atomic ratio of Co:B:Ni	Mass percentage of $Ni(OH)_2$
CoB	---	2.2:1	---
CoB@$Ni(OH)_2$	0.1	10.43:4.74:1	12.26 wt.%
CoB@$Ni(OH)_2$	0.14	5.89:2.68:1	19.79 wt.%
CoB@$Ni(OH)_2$	0.2	3.74:1.70:1	27.98 wt.%
CoB@$Ni(OH)_2$	0.26	3.88:1.85:1	27.28 wt.%

The bulk elemental compositions of CoB and CoB@$Ni(OH)_2$ samples determined by ICP are listed in Table S1. The mass percentage of $Ni(OH)_2$ in CoB@$Ni(OH)_2$ increased with the increase of the mole of the $NiCl_2$ precursor, and reaches the maxmium value of 27.98 wt.% at 0.2 moles of $NiCl_2$. Further increase of $NiCl_2$ reduced the $Ni(OH)_2$ loading content. As described above (see Material Synthesis), the formation of $Ni(OH)_2$ is two-stage, beginning with formation of metallic Co atoms. With the increase of $Ni(OH)_2$ loading, the thickness of the shell covers the available Co atoms thus preventing further reduction of Ni^{2+} to Ni metal.

Table S2. Comparison of CoB-core@$Ni(OH)_2$–shell with other core-$Ni(OH)_2$-shells reported in the literature .

Sample core-shell	Ref.	Specific capacitance (F g^{-1})	Areal capacitance (F cm^{-2})	[a]Current density	[b]Retention(%)/cycling number/[c]current density	Electrolyte
Chain-like CoB@Ni(OH) nanosheets	Our work	1293.7	7.76	2 A g^{-1}	85%/2500/2 A g^{-1}	6 M KOH
TiN nanowire arrays @gauze-like $Ni(OH)_2$	[1]	2680	---	6 A g^{-1}	16%/150/10 A g^{-1}	2 M KOH
SnO_2 nanowire arrays @$Ni(OH)_2$ ultrathin nanoflakes/Ni foam	[2]	1553	---	0.5 A g^{-1}	---	6 M KOH
Co_3O_4 nanowires @$Ni(OH)_2$ /Ni foam	[3]	1330	15.83	2.5 mA cm^{-2}	100%/1000/25mA cm^{-2}	6 M KOH
Fe_2O_3 nanowires @$Ni(OH)_2$ nanosheet/Fe foil	[4]	908	0.97	21.8 A g^{-1}	85.7%/5000/54.6 A g^{-1}	1 M NaOH
ZnO nanowires/$Ni(OH)_2$/textile fiber	[5]	3150	---	5 mV s^{-1}	98%/5000/20mV s^{-1}	1 M LiOH
Ni_3S_2 nanorod@$Ni(OH)_2$ nanosheet/graphene	[6]	1037	---	5.1 A g^{-1}	99.1%/2000/5.9 A g^{-1}	3 M KOH
$NiCo_2S_4$@$Ni(OH)_2$ nanotube arrays/carbon-fabric	[7]	2700	---	[d]1.3 A g^{-1}	78%/2000/5.9 A g^{-1}	1 M KOH
$NiMoO_4$@$Ni(OH)_2$ nanorods/Ni foams	[8]	4953	7.43	[d]2.7 A g^{-1}	72%/1000/16 A g^{-1}	2 M KOH
$ZnCo_2O_4$@$Ni(OH)_2$/Ni foam	[9]	2826	---	2 mA cm^{-2}	72%/2000/10mA cm^{-2}	3 M KOH
$NiCo_2O_4$@$Ni(OH)_2$/carbon fiber	[10]	2475	6.04	5 mA cm^{-2}	73.4%/1000/30mA cm^{-2}	2 M KOH

a: the specific capacitance and areal capacitance was obtained at the current density.
b: after cycling test, the retention of the specific capacitance.
c: the cycling test was carried out with the current density.
d: the value was calculated based on the data in the literature.

References:

[1] H. Yi, X. Chen, H. Wang, X. Wang, Electrochim. Acta 2014, 116, 372.

[2] Qingqing Ke, C. Guan, M. Zheng, Y. Hu, K.-h. Ho, J. Wang, Journal of Materials Chemistry A 2015, 3, 9538.

[3] C. H. Tang, X. Yin, H. Gong, ACS Appl. Mater. Interfaces 2013, 5, 10574.

[4] W. Tian, X. Wang, C. Zhi, T. Zhai, D. Liu, C. Zhang, D. Golberg, Y. Bando, Nano Energy 2013, 2, 754.

[5] I. Shakir, Z. Ali, J. Bae, J. Park, D. J. Kang, RSC Advances 2014, 4, 6324.

[6] W. Zhou, X. Cao, Z. Zeng, W. Shi, Y. Zhu, Q. Yan, H. Liu, J. Wang, H. Zhang, Energy Environ. Sci. 2013, 6, 2216.

[7] J. Zhang, H. Gao, M. Y. Zhang, Q. Yang, H. X. Chuo, Appl. Surf. Sci. 2015, 349, 870.

[8] Ge Jiang, Mingyi Zhang, Xueqing Li, Hong Gao, RSC Advances 2015, 5, 69365.

[9] H. X. Chuo, H. Gao, Q. Yang, N. Zhang, W. B. Bu, X. T. Zhang, Journal of Materials Chemistry A 2014, 2, 20462.

[10] W. Li, L. Xin, X. Xu, Q. Liu, M. Zhang, S. Ding, M. Zhao, X. Lou, Sci Rep 2015, 5, 9277.